



# 100 kyr fluvial cut-and-fill terrace cycles since the Middle Pleistocene in the southern Central Andes, NW Argentina



Stefanie Tofelde<sup>a,b,\*</sup>, Taylor F. Schildgen<sup>a,b</sup>, Sara Savi<sup>a</sup>, Heiko Pingel<sup>a</sup>, Andrew D. Wickert<sup>c</sup>, Bodo Bookhagen<sup>a</sup>, Hella Wittmann<sup>b</sup>, Ricardo N. Alonso<sup>d</sup>, John Cottle<sup>e</sup>, Manfred R. Strecker<sup>a</sup>

<sup>a</sup> Institut für Erd- und Umweltwissenschaften, Universität Potsdam, 14476 Potsdam, Germany

<sup>b</sup> Helmholtz-Zentrum Potsdam, Deutsches GeoForschungsZentrum (GFZ) Potsdam, 14473 Potsdam, Germany

<sup>c</sup> Department of Earth Sciences and Saint Anthony Falls Laboratory, University of Minnesota, Minneapolis, MN 55455, USA

<sup>d</sup> Departamento de Geología, Universidad Nacional de Salta and CONICET (CEGA-INSUGEO), 4400 Salta, Argentina

<sup>e</sup> Department of Earth Science and Earth Research Institute, University of California, Santa Barbara, CA 93106, USA

## ARTICLE INFO

### Article history:

Received 1 February 2017

Received in revised form 31 May 2017

Accepted 1 June 2017

Available online xxx

Editor: A. Yin

### Keywords:

<sup>10</sup>Be depth-profiles

surface inflation

aggradation–incision cycles

glacial–interglacial cycles

landscape response to climate change

Eastern Cordillera

## ABSTRACT

Fluvial fill terraces in intermontane basins are valuable geomorphic archives that can record tectonically and/or climatically driven changes of the Earth-surface process system. However, often the preservation of fill terrace sequences is incomplete and/or they may form far away from their source areas, complicating the identification of causal links between forcing mechanisms and landscape response, especially over multi-millennial timescales. The intermontane Toro Basin in the southern Central Andes exhibits at least five generations of fluvial terraces that have been sculpted into several-hundred-meter-thick Quaternary valley-fill conglomerates. New surface-exposure dating using nine cosmogenic <sup>10</sup>Be depth profiles reveals the successive abandonment of these terraces with a 100 kyr cyclicity between  $75 \pm 7$  and  $487 \pm 34$  ka. Depositional ages of the conglomerates, determined by four <sup>26</sup>Al/<sup>10</sup>Be burial samples and U–Pb zircon ages of three intercalated volcanic ash beds, range from  $18 \pm 141$  to  $936 \pm 170$  ka, indicating that there were multiple cut-and-fill episodes. Although the initial onset of aggradation at  $\sim 1$  Ma and the overall net incision since ca. 500 ka can be linked to tectonic processes at the narrow basin outlet, the superimposed 100 kyr cycles of aggradation and incision are best explained by eccentricity-driven climate change. Within these cycles, the onset of river incision can be correlated with global cold periods and enhanced humid phases recorded in paleoclimate archives on the adjacent Bolivian Altiplano, whereas deposition occurred mainly during more arid phases on the Altiplano and global interglacial periods. We suggest that enhanced runoff during global cold phases – due to increased regional precipitation rates, reduced evapotranspiration, or both – resulted in an increased sediment-transport capacity in the Toro Basin, which outweighed any possible increases in upstream sediment supply and thus triggered incision. Compared with two nearby basins that record precessional (21-kyr) and long-eccentricity (400-kyr) forcing within sedimentary and geomorphic archives, the recorded cyclicity scales with the square of the drainage basin length.

© 2017 Elsevier B.V. All rights reserved.

## 1. Introduction

Mountain belts are continually reshaped by Earth-surface processes that erode, transiently store, and transport sediment to foreland regions and beyond (e.g., Allen, 2008). This sediment transport system responds to perturbations in climate and tectonics, and thus has varied significantly during the Cenozoic. However,

most of our understanding of sediment source-to-sink dynamics in the past is based on sedimentary archives that are often located far from their source areas, such that temporal buffering of the sediment transport complicates a direct correlation with a particular external forcing mechanism (Castelltort and Van Den Driessche, 2003). Despite major advances in understanding the timing of past climatic changes during the Quaternary, our knowledge about how (often cyclic) changes in environmental conditions are reflected and preserved in terrestrial landscapes is still limited (Braun et al., 2015; Castelltort and Van Den Driessche, 2003; Godard et al., 2013).

\* Corresponding author at: Institut für Erd- und Umweltwissenschaften, Universität Potsdam, 14476 Potsdam, Germany.

E-mail address: tofelde@uni-potsdam.de (S. Tofelde).

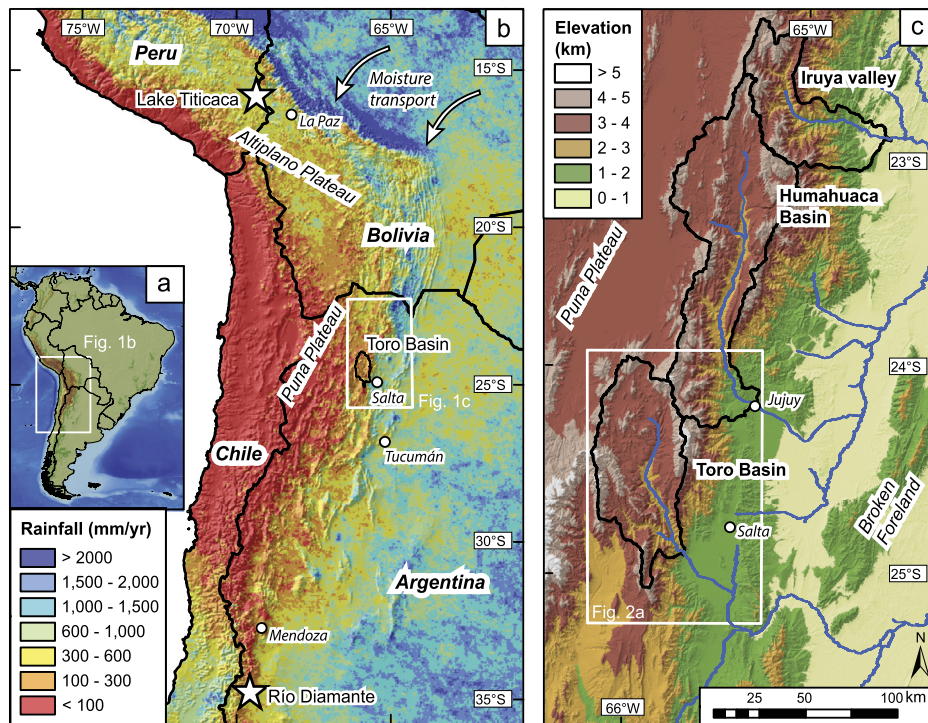


**Fig. 1.** Rainfall of the Central Andes and regional topography of NW Argentina. (a) Map of South America. White box shows outline of (b). (b) Rainfall map calculated from TRMM2B31 product with a 5 km resolution (Bookhagen and Strecker, 2008). Stars mark Lake Titicaca – a paleo climate record site (Fritz et al., 2007) and Río Diamante – a site of dated fluvial fill terraces that cover several glacial–interglacial cycles (Baker et al., 2009). (c) Topography from SRTM dataset (~30 m resolution; data available from the U.S. Geological Survey). Black lines delineate the catchments of the Toro Basin, Humahuaca Basin and Iruya valley.

Fluvial fill terraces offer potential insights into this problem, as they record changes in sediment flux ( $Q_s$ ) and/or water discharge ( $Q_w$ ) over time. As early as 1884, A. Penck correlated river terraces in the European Alpine foreland with glacial advance and retreat in the mountains (Penck, 1884). Based on multiple fluvial terrace sequences in the arid interior of Central Asia, Huntington (1907) suggested a close link between increased hillslope erosion, reduced vegetation cover, and aggradation during arid conditions, followed by incision during humid phases. Since then, studies from around the globe have linked fluvial fill terrace formation in glaciated catchments with variability in  $Q_s$  and  $Q_w$  over glacial–interglacial cycles (e.g. Bridgland and Westaway, 2008; Huang et al., 2014; Pan et al., 2003; Wegmann and Pazzaglia, 2009). Little is known, however, about how variability in global climate may have affected Earth-surface processes on multi-millennial timescales in regions far from major glaciers and ice sheets, and how those changes might be reflected in the landscape.

High-altitude moraines indicate the presence of past glaciers in the Central Andes (Haselton et al., 2002; Zech et al., 2009). Even in areas without extensive past ice cover, multiple levels of fluvial terraces in the Central Andes have been described (e.g., Baker et al., 2009; Farabaugh and Rigsby, 2005; Schildgen et al., 2016; Steffen et al., 2010; Tchilinguirian and Pereyra, 2001). Where dated, the terraces mainly span the last glacial–interglacial cycle (Farabaugh and Rigsby, 2005; Schildgen et al., 2016; Steffen et al., 2010); terraces spanning timescales longer than 120 kyr have only been reported in one study from the Andes – along the Río Diamante (Fig. 1b; Baker et al., 2009).

The Toro Basin in the Central Andes of NW Argentina (Fig. 1) contains several hundred meters of sub-horizontal conglomerates deposited after 0.98 Ma (Marrett et al., 1994) that have been incised by the Río Toro to create multiple terrace levels. These terraces are located high in the basin, proximal to the source area, offering a rare opportunity to study the sediment routing system before sediment storage and re-mobilization buffer the signal. To

better understand the dynamics of the sediment transport system within this intermontane basin, we determined the onset of river-incision phases by dating the exposure of the three most extensive and best-preserved terrace surfaces (treads) with cosmogenic  $^{10}\text{Be}$  depth profiles. The timing of depositional events is based on cosmogenic burial dating and U–Pb zircon dating of volcanic ashes that are incorporated into the fill material. Based on the chronology we derive from these data, we consider the potential impact of autogenic forcing, tectonics, and climate variability on the evolution of the valley fill.

## 2. Study area

### 2.1. Geological and geomorphic setting

The Central Andean Plateau is subdivided into a northern (Altiplano) and a southern (Puna) sector (Fig. 1b). The Toro Basin at ~24.5°S is one of several intermontane basins located in transition between the high-elevation, arid Puna to the west and the low-elevation, humid foreland to the east (Fig. 1c).

The basin is confined by reverse-fault bounded basement ranges, namely the Cumbres de Zamanca and Sierra de Almagro to the west and the Sierra de Pascha and the Sierra de Pascha Sur to the east (Fig. 2a). The main basin-bounding faults are the west-dipping Solá Fault to the west, the northwest-dipping San Bernardo Fault to the north, and the east-dipping Gólgota Fault to the east (Marrett and Strecker, 2000). The Solá Fault has been active at least since the Pliocene, and deformation along the San Bernardo and Gólgota faults extends from the Miocene until at least 0.98 Ma (Marrett and Strecker, 2000), with potential re-activation of the Gólgota Fault after 0.98 Ma (Hilley and Strecker, 2005). Exposed basement rocks mainly comprise quartz-bearing meta-sediments of the Late Proterozoic to Cambrian Puncoviscana Formation and Paleozoic quartzites and shales of the Mesón group (Schwab and Schäfer, 1976).

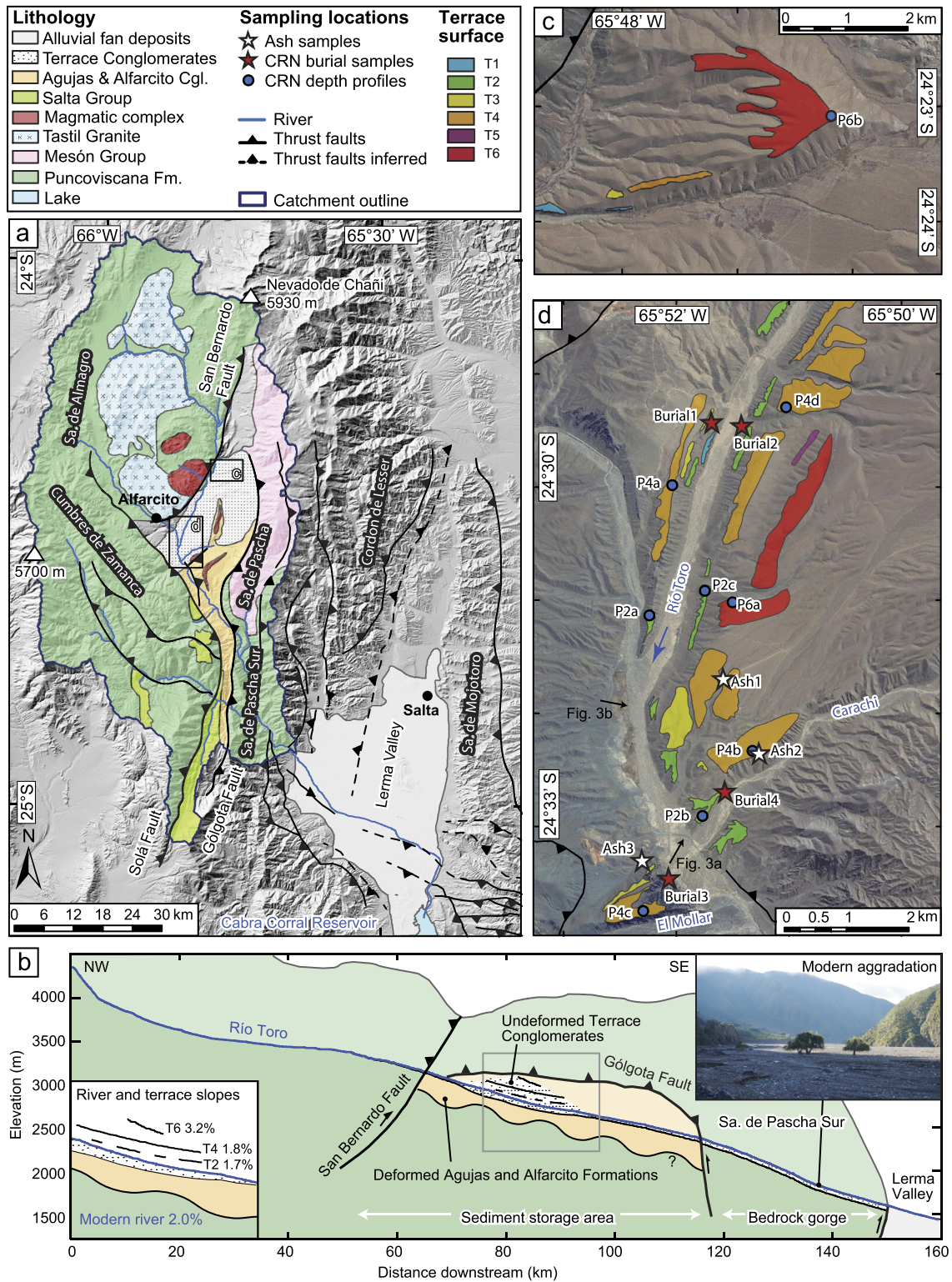


**Fig. 2.** Detailed overview of the Toro Basin and the fill terraces. (a) Geological map of the Toro Basin and northern part of the Lerma Valley based on previous work by García et al. (2013) and Hilley and Strecker (2005). (b) Longitudinal profile of the Río Toro with projected lithological and structural interpretations. Left insert: Slopes of the modern river and of three out of six terraces. The terrace slopes were estimated based on differential GPS measurements and SRTM data. Right insert: Field photograph showing modern sediment aggradation of the riverbed. Note the buried trees. (c) and (d) ArcGIS Basemap imagery including sample locations and mapped terrace levels. Black arrows in (d) indicate direction of field photos shown in Fig. 3a and b. Abbreviations: Cgl. = Conglomerates, Fm. = Formation, Sa. = Sierra.

Whereas the morphology of the southern part of the basin is dominated by a narrow bedrock gorge presently experiencing sediment aggradation (Fig. 2b), the region upstream of the Gólgota Fault is a low-relief landscape, where most of the late Cenozoic

sedimentary basin deposits are stored. The Toro Basin is drained by the perennial, braided Río Toro, which flows with a mean gradient of ~1.6% between the upper end of the terrace deposits and the lower end of the bedrock gorge. At the outlet of the gorge, a frac-

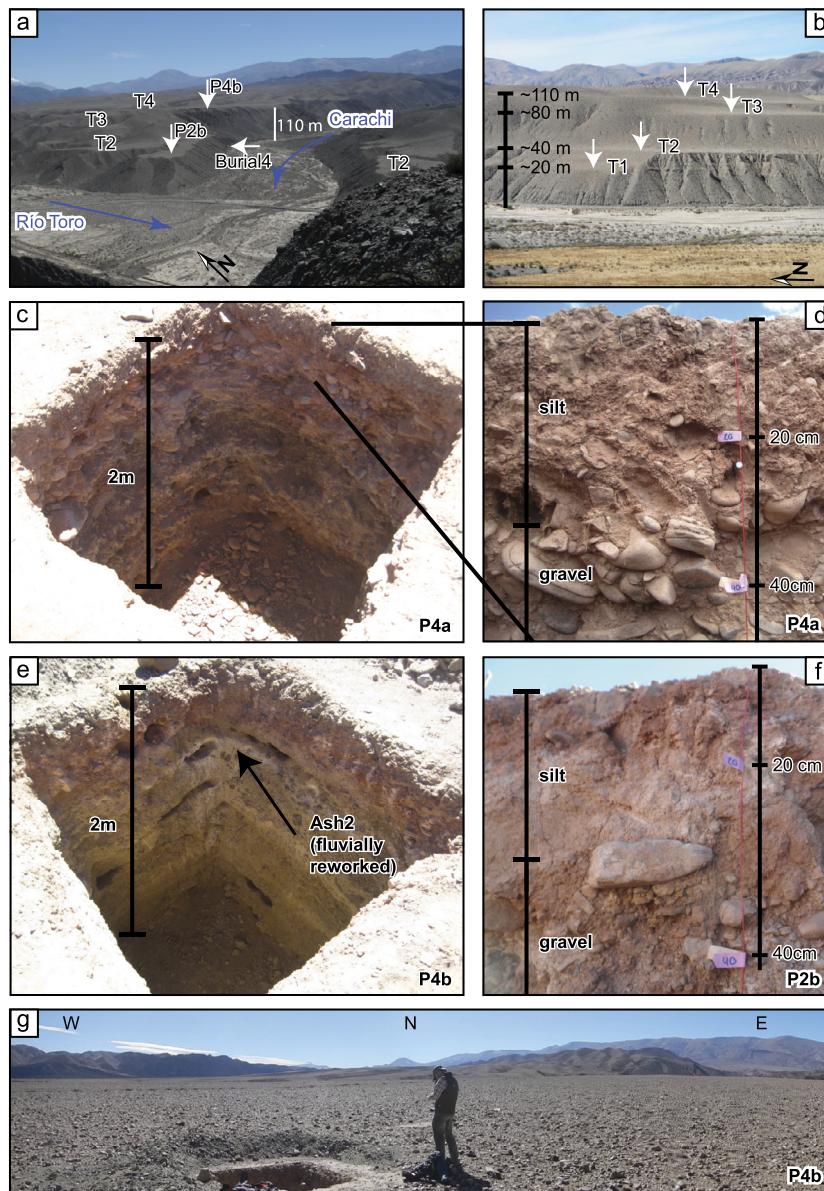


**Fig. 3.** Field pictures of the Terrace Conglomerates. (a) Fluvial fill terraces at a confluence and (b) along the Río Toro main-channel. The locations of the terrace field photos are indicated by arrows in Fig. 2d. The pits for  $^{10}\text{Be}$  depth profiles (c, e) were excavated on terrace surfaces far from the terrace margins and slopes of nearby terraces to avoid erosion or potential overwash. Within the pits seven to eight samples for  $^{10}\text{Be}$  depth profile analysis were collected. Close-ups of the upper 40 cm of P4a (d) and P2b (f). A fine sand to silt layer can be distinguished from underlying gravel – a feature commonly observed in desert pavements (McFadden et al., 1987); same as the layer of closely packed, interlocking clast at the surface (g). The fine sand to silt layer in desert pavements is related to aeolian input and causes inflation of the surfaces over time.

tion of the sediment removed from the Toro Basin is re-deposited on an alluvial fan in the Lerma Valley (Fig. 2a).

Hilley and Strecker (2005) suggested that the oscillatory character of the sediment deposition and excavation in the Toro Basin, comprising at least two periods of filling and excavation since 8 Ma, is related to the interplay between rock uplift, rock type, and climate. The eroded and tilted Alfarcito conglomerates document an initial basin-filling stage. After 0.98 Ma, the Toro Basin was excavated to a base level lower than today. It was subsequently re-filled by a several-hundred-meter thick, sub-horizontal conglomeratic unit (“Terrace Conglomerates”) (Fig. 2a and b) (Hilley and Strecker, 2005; Marrett and Strecker, 2000). Hilley and Strecker (2005) suggested that this valley fill resulted from reactivated uplift of the Sierra de Pascha Sur after 0.98 Ma, a basement block bounded to the west by the Gólgota Fault and to the east by a less pronounced fault at the basin outlet. The mechanically strong basement rock of the Sierra de Pascha Sur could not be incised

as quickly as it was uplifted, which led to aggradation upstream of the Gólgota Fault and channel steepening within the gorge (Fig. 2b). The resultant post-0.98 Ma Terrace Conglomerates overlie tectonically-deformed and eroded paleo-topography. This conglomerate was then incised, leaving behind a flight of at least five to six paired terrace levels (one surface is only visible in one location as small remnants) between 20 and 220 m above the present-day river (Fig. 3a and b) (Hilley and Strecker, 2005; Marrett and Strecker, 2000; Schwab and Schäfer, 1976). The stratigraphy of the un lithified, sub-horizontal Terrace Conglomerates does not reveal distinct units. Therefore, it is unclear whether the Terrace Conglomerates consist of one fill unit followed by stepwise incision or if each terrace is related to one cut-and-fill cycle.

The Terrace Conglomerates are clast-supported, pebble to cobble conglomerates that consist of well-rounded, often imbricated, and partly sorted clasts, commonly up to several decimeters in diameter, with rare boulders. The gently inclined terraces are capped

by desert pavements (Fig. 3), characterized by closely packed, interlocking clasts that overlie a layer of fine sand and silt (e.g., McFadden et al., 1987), which in turn covers the conglomerates. The thickness of these fine sand/silt layers varies among the surfaces from 10 to 50 cm, with the higher terraces generally having a greater thickness.

## 2.2. Climatic setting

The eastern flanks of the southern Central Andes of Argentina (including the intermontane basins of the Eastern Cordillera) are characterized by pronounced orographic rainfall gradients (Fig. 1b, Bookhagen and Strecker, 2008). Water vapor transport from the Atlantic Ocean and Amazon Basin is mainly governed by the South American Summer Monsoon (SASM) system, in which the South American low-level jet (SALLJ) funnels air masses southward along the Andes into (sub-)tropical South America (Castino et al., 2016; Vera et al., 2006). The Toro Basin, situated at the southern end of the SALLJ conveyor, receives rainfall ranging from ~900 mm/yr at the outlet to <200 mm/yr in the interior of the basin.

Moisture supplied to the Central Andes has varied significantly over the past several tens of thousands of years (see review by Baker and Fritz, 2015). Variability in the intensity of SASM precipitation on precessional timescales (21 kyr) has been documented by paleo-lake studies on the Puna Plateau of Argentina and Chile (Bobst et al., 2001; Godfrey et al., 2003) and the Bolivian Altiplano (Titicaca Basin: Fritz et al., 2010; Uyuni Basin: Fritz et al., 2004; Placzek et al., 2006). During cold periods in the Northern Hemisphere, the Atlantic portion of the intertropical convergence zone (ITCZ) was displaced southward and caused corresponding shifts of the moisture-bearing wind systems (Broccoli et al., 2006). The enhancement of rainfall in the Central Andes during these cold phases provided the necessary moisture for glacier growth and higher lake levels (Haselton et al., 2002; Vizy and Cook, 2007). An overall increase in moisture supply to the Altiplano during colder phases also occurred on ~100 kyr (eccentricity) cycles. Near Lake Titicaca (Fig. 1b), increased pollen abundance of aquatic species and green algae (Gosling et al., 2008) as well as lake highstands (Fritz et al., 2007) correlate with regional glacial advances and global glacial stages.

At present, the high ranges surrounding the Toro Basin are not glaciated. However, glacial landforms and multiple generations of moraines above 3800 m elevation document previous glacial activity in the region, with an estimated cover of less than 5% of the Toro Basin.

## 3. Methods

To determine the onset of incision phases of the Terrace Conglomerates, we applied cosmogenic radionuclide (CRN) exposure dating to the terrace treads. The timing of aggradation was identified based on  $^{26}\text{Al}/^{10}\text{Be}$  burial dating and U–Pb zircon dating of intercalated, Puna-derived volcanic ash deposits. Fluvial terraces were mapped in the field with GPS and correlated using aerial and satellite imagery based on their elevation above the modern channel.

### 3.1. Cosmogenic radionuclide dating

Exposure ages of the most prominent terrace treads were derived from *in situ* cosmogenic  $^{10}\text{Be}$  depth profiles collected from newly dug pits. The *in situ* production of  $^{10}\text{Be}$  is highest at the Earth's surface and decreases approximately exponentially with depth (Lal, 1991). Hence, exponential curve fitting of a suite of measured  $^{10}\text{Be}$  concentrations from a vertical profile can reveal the most likely surface and inherited concentrations (Anderson et al.,

1996). The latter comprises  $^{10}\text{Be}$  accumulated prior to deposition (during exhumation and transport), and is assumed to be uniform with depth. After subtracting the inheritance from the surface concentration, the remaining  $^{10}\text{Be}$  concentration is used to calculate a surface-exposure age.

Depth profiles P2a, P2b, P4a, P4b and P4c were sampled in 2014, whereas P2c, P4d, P6a and P6b were sampled in 2003. In the profile names, “P” indicates a depth profile, numbers refer to the corresponding terrace (T1 through T6 from low to high elevation), and the final letter distinguishes multiple profiles from the same terrace (a–d). To ensure a minimal influence of terrace modification (erosion or burial) on calculated ages, the location of each depth profile was chosen several tens of meters from the closest terrace edge (Fig. 3g). Each depth profile from 2014 consists of seven to eight samples collected over a depth range of 2 to 5 m below the surface, with each sample comprising material collected over a ca. 10 to 20 cm depth interval (Table S1). Due to the available material, samples from profiles P2b, P4a and P4c comprise 60–100 amalgamated pebbles (1–3 cm diameter), whereas those from P2a and P4b comprise sand. The depth profiles from 2003 consist of five to seven samples each, collected over a depth range of 2.5 m (Table S1). Each sample comprises 20 to 30 pebbles (3–5 cm diameter) collected over a depth interval of up to 50 cm.

Additionally, we dated the timing of sediment burial based on  $^{26}\text{Al}/^{10}\text{Be}$  ratios of sand samples (e.g., Granger and Muzikar, 2001) collected in 2015 (Fig. 2d, Table S2). Because the decay constant of  $^{26}\text{Al}$  ( $\lambda_{\text{Al}} = 9.83 \pm 0.25 \times 10^{-7} \text{ yr}^{-1}$ ) (Nishiizumi, 2004) is nearly twice as high as that of  $^{10}\text{Be}$  ( $\lambda_{\text{Be}} = 4.99 \pm 0.043 \times 10^{-7} \text{ yr}^{-1}$ ) (e.g., Chmeleff et al., 2010), the initial surface nuclide ratio of  $^{26}\text{Al}/^{10}\text{Be} = 6.75$  (Balco and Shuster, 2009) decreases with time after burial. To minimize effects of post-burial CRN production, we collected the four burial samples at locations that were shielded by at least 10 m of sediment cover (Fig. S1). This approach restricted us to sampling only a few feasible sites.

All CRN samples collected in 2003 were processed at the Space Science Laboratory (UC Berkeley, USA), with AMS measurements performed at Lawrence Livermore National Laboratory (USA). The samples collected in 2014 and 2015 were processed both at the University of Potsdam and GeoForschungsZentrum Potsdam (Germany), with AMS measurements performed at the University of Cologne (Germany). The sample preparation followed standard procedures; a detailed description is provided in the supplementary material.

Terrace tread exposure ages were determined using a combination of a Monte Carlo simulator (Hidy et al., 2010) and the CRONUS Earth online calculator v2.2 (Balco et al., 2008). We adjusted the Monte Carlo simulator to allow for this combined approach (see supplementary material). All CRN calculations were performed with the regional reference production rate from Blard et al. (2013) ( $3.79 \pm 0.23 \text{ atm g}^{-1} \text{ yr}^{-1}$ ) and the time-dependent (“Lm”) (Balco et al., 2008) scaling scheme.

### 3.2. U–Pb zircon geochronology

We dated three intercalated volcanic ashes to support cosmogenic burial dating constrains on the timing of conglomerate deposition. Zircon grains were extracted using standard magnetic and heavy liquid methods, handpicked, mounted in epoxy, and polished for U, Th, and Pb isotope analysis using a Laser Ablation Multi-Collector Inductively Coupled Plasma Mass Spectrometer (LA-MC-ICPMS) at the University of California, Santa Barbara. Due to significant pre-eruption residence times and/or post-eruptive reworking, analyzed samples show a wide distribution of  $^{206}\text{Pb}/^{238}\text{U}$  zircon ages. Therefore, we systematically excluded the oldest ages from our calculations of an average zircon crystallization age until near-unity values for the mean square of weighted deviates (MSWD <

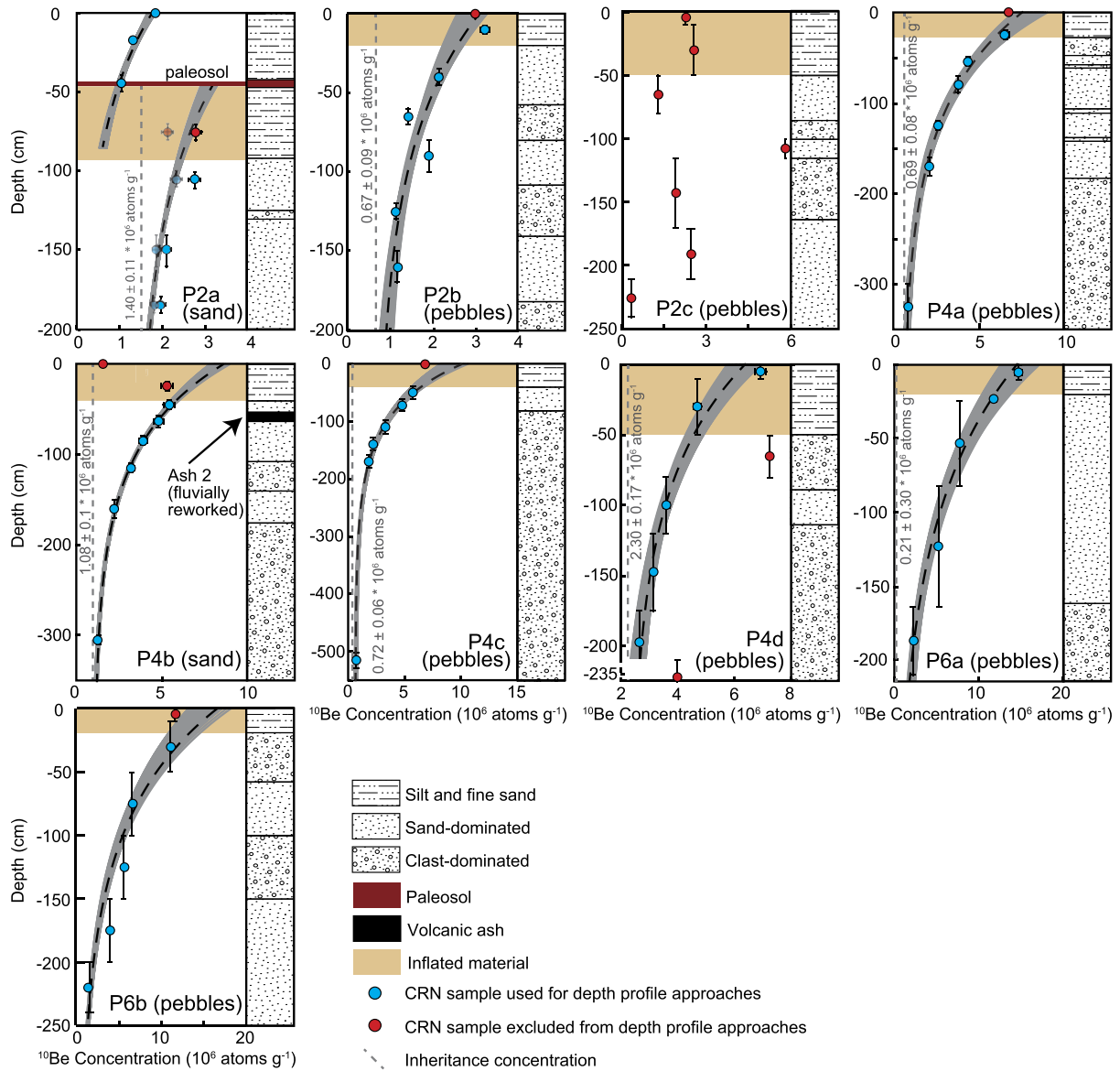


**Fig. 4.** Distribution of  $^{10}\text{Be}$  concentration with depth for the nine profiles and sedimentary logs of the sampled pit walls. Areas shaded in light brown indicate the silt/fine sand layer observed at the top of each profile. Within each profile we either sampled exclusively sand or pebbles. Each sample was collected over a vertical depth range indicated by the vertical error bar. The horizontal error bar represent the  $1\sigma$  analytical uncertainty. Samples marked in blue were included for the *Stable-surface* approach and the *Inflation-corrected* approach (Fig. S2), while red samples were excluded. The red surface samples were used for the *Surface-pebbles* approach instead. For P2a the top and lower part were considered as two individual profiles. For the lower profile we corrected the concentration for the time of burial by the top unit (transparent circles). We used the Monte Carlo simulator (Hidy et al., 2010) to fit 50,000 curves to each profile (grey), resulting in a most-probable fit (black dashed curve).

2) were achieved. Where no coherent population was found, we selected the youngest  $^{206}\text{Pb}/^{238}\text{U}$  zircon ages to represent a maximum depositional age. All analytical results and further methodological information can be found in the supplementary material.

## 4. Results

### 4.1. Terrace tread exposure dating

Out of six observed terrace levels in the Toro Basin (T1–T6), we determined exposure ages of the three most extensive and best-preserved treads (T2, T4 and T6). On each selected terrace, we sampled between two and four depth profiles for cosmogenic  $^{10}\text{Be}$  analyses (Fig. 2c and d, Table S1).

In general,  $^{10}\text{Be}$  concentrations from the depth profiles decrease exponentially with depth, except for P2c, which does not show any correlation with depth, and P2a, which appears to have two ex-

ponential trends separated by a thin paleosol at  $\sim 45$  cm depth (Fig. 4). In several cases (P2a, P2b, P4a, P4b, P4c and P6a), the surface samples have a  $^{10}\text{Be}$  concentration that falls below the expected exponential pattern (red circles in Fig. 4); this is also the case for the shallow subsurface sample in P4b. These samples all fall within the layer of fine sand/silt (see section 2.1 and Fig. 3). Although these samples may be outliers, another explanation is dilution of the originally deposited material with aeolian fine sand and silt. During desert pavement formation, aeolian material accumulates beneath and inflates the upper clast layer (e.g., McFadden et al., 1987). To account for potential inflation of desert-pavement surfaces, we pursued three different approaches for each depth profile to calculate the terrace-surface exposure ages. We term these (1) the *Stable-surface* approach, (2) the *Inflation-corrected* approach, and (3) the *Surface-pebbles* approach (for a summary see Fig. S2).

**Table 1**

Summary of terrace surface exposure ages based on the three different approaches. The standard deviation ( $1\sigma$ ) for the depth profiles includes the uncertainty in the surface concentration (outcome of Monte Carlo fits), the uncertainties of the local production rate and of the  $^{10}\text{Be}$  decay constant. The standard deviation for the surface pebbles samples is the external uncertainty given by the CRONUS calculator. The CRONUS input included the analytical uncertainty of the surface sample as well as the uncertainty of the predicted inheritance. Ages in bold we consider as most reliable and are plotted in Fig. 6d as light blue lines.

Sample name (Inflation in cm)	Terrace level	(1) Stable-surface (ka $\pm 1\sigma$ )	(2) Inflation-corrected (ka $\pm 1\sigma$ )	(3) Surface-pebbles (ka $\pm 1\sigma$ )
P2a (40–45)	T2	153 <sup>+14</sup> / <sub>-17</sub>	<b>133<sup>+12</sup>/<sub>-11</sub></b>	
P2a (top only)	T2	<b>75<sup>+4</sup>/<sub>-7</sub></b>		
P2b (20–22)	T2	104 <sup>+10</sup> / <sub>-11</sub>	93 <sup>+9</sup> / <sub>-9</sub>	<b>108 <math>\pm</math> 9</b>
P2c	T2	–	–	<b>85 <math>\pm</math> 8</b>
P4a (20–25)	T4	319 <sup>+23</sup> / <sub>-22</sub>	282 <sup>+20</sup> / <sub>-20</sub>	<b>269 <math>\pm</math> 20</b>
P4b (30–40)	T4	327 <sup>+25</sup> / <sub>-22</sub>	266 <sup>+20</sup> / <sub>-20</sub>	
P4c (30–50)	T4	411 <sup>+32</sup> / <sub>-34</sub>	307 <sup>+28</sup> / <sub>-24</sub>	<b>284 <math>\pm</math> 26</b>
P4d (45–50)	T4	164 <sup>+12</sup> / <sub>-17</sub>	121 <sup>+11</sup> / <sub>-11</sub>	190 $\pm$ 14/ <b>263 <math>\pm</math> 18</b>
P6a (18–22)	T6	732 <sup>+53</sup> / <sub>-56</sub>	644 <sup>+43</sup> / <sub>-49</sub>	<b>487 <math>\pm</math> 34</b>
P6b (22–24)	T6	406 <sup>+26</sup> / <sub>-28</sub>	358 <sup>+21</sup> / <sub>-26</sub>	<b>453 <math>\pm</math> 33</b>

In the *Stable-surface* and *Inflation-corrected* approaches, we removed the uppermost low-concentration samples from the profiles (red circles in Fig. 4) and performed exposure-age calculations based on curve-fitting to the remaining samples. The *Stable-surface* approach assumes no inflation of the terrace surface over time (although total erosion is allowed to vary between  $\pm 1$  cm), whereas in the *Inflation-corrected* approach, we simulated the accumulation of the fine sand/silt layer in the upper part of the profiles over time. In the *Surface-pebbles* approach, we subtracted the most-probable inherited  $^{10}\text{Be}$  concentration derived from the depth profiles from the surface samples (the ones that were excluded from the first two approaches; red circles in Fig. 4) and then calculated exposure ages from the remaining  $^{10}\text{Be}$  concentration.

Ages derived from the *Stable-surface* and *Inflation-corrected* approaches range from 75<sup>+4</sup>/<sub>-7</sub> and 732<sup>+53</sup>/<sub>-56</sub> ka and are reported with  $1\sigma$  uncertainty (Table 1; details in Table S5 and Fig. S3). When comparing the two sets of results, the *Inflation-corrected* ages are younger by 11% (P2b) to 26% (P4d).

The *Surface-pebbles* approach was only applied to the pebble profiles. Because the  $^{10}\text{Be}$  concentration in the surface-pebble sample is insensitive to dilution by aeolian material, it allows us to test the inflation hypothesis. The resulting ages range from 85  $\pm$  8 ka to 487  $\pm$  34 ka (Table 1, details in Table S7).

A sub-set of the profiles required modifications in our approaches. When applying the *Stable-surface* and *Inflation-corrected* approaches to profile P2a, we infer that the two exponential trends define two depositional events separated by a period of exposure as indicated by the formation of a paleosol. For the upper fill, we calculated a surface-exposure age of 75<sup>+4</sup>/<sub>-7</sub> ka. To calculate the exposure age for the lower fill, we first subtracted the amount of  $^{10}\text{Be}$  produced in the samples of the lower fill unit since the deposition of the upper fill unit. Based on the remaining  $^{10}\text{Be}$  concentration (Fig. 4, transparent circles in P2a), we calculated a surface exposure duration for the lower unit. The exposure duration is 78<sup>+12</sup>/<sub>-15</sub> ka for the *Stable-surface* approach or 58<sup>+11</sup>/<sub>-8</sub> ka for the *Inflation-corrected* approach. Thus, the addition of the exposure duration of the lower surface to the exposure age of the upper surface implies that the lower surface was exposed at either 153<sup>+14</sup>/<sub>-17</sub> ka (*Stable-surface*) or at 133<sup>+12</sup>/<sub>-11</sub> ka (*Inflation-corrected*).

For three profiles (P6a, P2c and P4d) we needed to adjust the *Surface-pebbles* approach due to insufficiently constrained  $^{10}\text{Be}$  inheritance concentrations. For P6a, the depth-profile fits suggested no inheritance, and for P2c, we could not find any depth profile fits. Therefore, for both profiles, we assumed that the inheritance is equal to the concentration of the lowermost sample in the profile, and thus we obtained ages of 487  $\pm$  34 ka and 85  $\pm$  8 ka, respec-

tively. We performed two calculations using the *Surface-pebbles* approach for P4d: one with the calculated inheritance from P4d (*P4d\_surf\_4d* in Table S7) and one with the calculated inheritance from P4a (*P4d\_surf\_4a*), which is located on the same terrace level and received material from the same catchment. The two resulting exposure ages are 190  $\pm$  14 ka and 263  $\pm$  18 ka, respectively.

#### 4.2. Depositional ages

To clarify whether the conglomeratic fill of the Toro Basin was emplaced during a single depositional episode and was later incrementally incised, or if it records multiple cut-and-fill cycles, we determined four CRN burial ages (Fig. 2d, Table S2). *Burial1* was sampled from the fill unit below T3. *Burial2* and *Burial4* were sampled from material below T2, with *Burial2* containing sands derived from the Toro main stem, whereas *Burial4* sands were transported by the Carachi tributary river (Fig. 2d and 3a). *Burial3* was located below T4, but sampled at the exposed base of the fill unit.  $^{26}\text{Al}/^{10}\text{Be}$  ratios of 6.69  $\pm$  0.07, 5.82  $\pm$  0.06, 4.29  $\pm$  0.08 and 5.77  $\pm$  0.06 yield burial ages of 18  $\pm$  141 ka (*Burial1*), 306  $\pm$  125 ka (*Burial2*), 936  $\pm$  170 ka (*Burial3*) and 325  $\pm$  130 ka (*Burial4*) (Table 2; ages given with  $1\sigma$  uncertainty).

In addition to the burial ages, we obtained three U–Pb zircon ages from intercalated volcanic ash layers in the Terrace Conglomerates (Fig. 2d, Table S8). *Ash1* is from a several dm thick, fluvially reworked ash layer that was sampled a few centimeters below the surface of T4 and yielded a maximum depositional age of 269  $\pm$  30 ka ( $n = 2/49$ ;  $2\sigma$  uncertainty). *Ash2* from within P4b on T4 is also reworked, but much less pronounced than *Ash1*. It was deposited around fluvially transported clasts (Fig. 3e) and yielded a maximum depositional age of 417  $\pm$  38 ka ( $n = 2/60$ ). Finally, *Ash3* was collected from a prominent ash layer in fill material north of the El Mollar tributary. Although terrace surfaces are not well preserved in this location, the elevation above the current river suggests that the ash-bearing material belongs to the fill material below T3. This sample yielded a consistent age population of 218  $\pm$  14 ka (MSWD = 1.48;  $n = 14/60$ ).

## 5. Discussion

### 5.1. Reliability and interpretation of terrace exposure ages

A comparison of the three different approaches to calculate terrace-surface exposure ages (Table 1) reveals that (a) the exposure ages vary significantly depending on the chosen approach (e.g. including inflation or not) and (b) ages from the *Surface-pebbles* approach generally agree better with the *Inflation-corrected* ages than

**Table 2**  
Burial ages based on paired  $^{10}\text{Be}$  and  $^{26}\text{Al}$  measurements. For the calculations we assumed a constant surface production ratio of  $^{26}\text{Al}/^{10}\text{Be} = 6.75$ , an  $^{26}\text{Al}$  decay constant of  $\lambda_{\text{Al}} = 9.38 \times 10^{-7}$  (Nishiizumi, 2004) and a  $^{10}\text{Be}$  decay constant of  $\lambda_{\text{Be}} = 4.987 \times 10^{-7}$  (e.g., Chmeleff et al., 2010). Burial age uncertainties include measurement and decay-constant uncertainties. Ages in bold we consider as most reliable and are plotted in Fig. 6e as solid red lines.

Sample name	Calculated $^{10}\text{Be}$ concentration ( $^{10}\text{Be}$ atm $\text{g}^{-1} \pm 1\sigma$ )		Calculated $^{26}\text{Al}$ concentration ( $^{26}\text{Al}$ atm $\text{g}^{-1} \pm 1\sigma$ )		$^{26}\text{Al}/^{10}\text{Be}$ ratio	Burial age (ka $\pm 1\sigma$ )
Burial 1	7.21E+05±	3.86E+04	4.82E+06±	2.04E+05	6.69 ± 0.07	18 ± 141
Burial 2	8.05E+05±	2.57E+04	4.69E+06±	2.37E+05	5.82 ± 0.06	<b>306 ± 125</b>
Burial 3	1.71E+05±	6.56E+03	7.34E+05±	5.07E+04	4.29 ± 0.08	<b>936 ± 170</b>
Burial 4	2.91E+05±	1.02E+04	1.68E+06±	8.72E+04	5.77 ± 0.06	<b>325 ± 130</b>

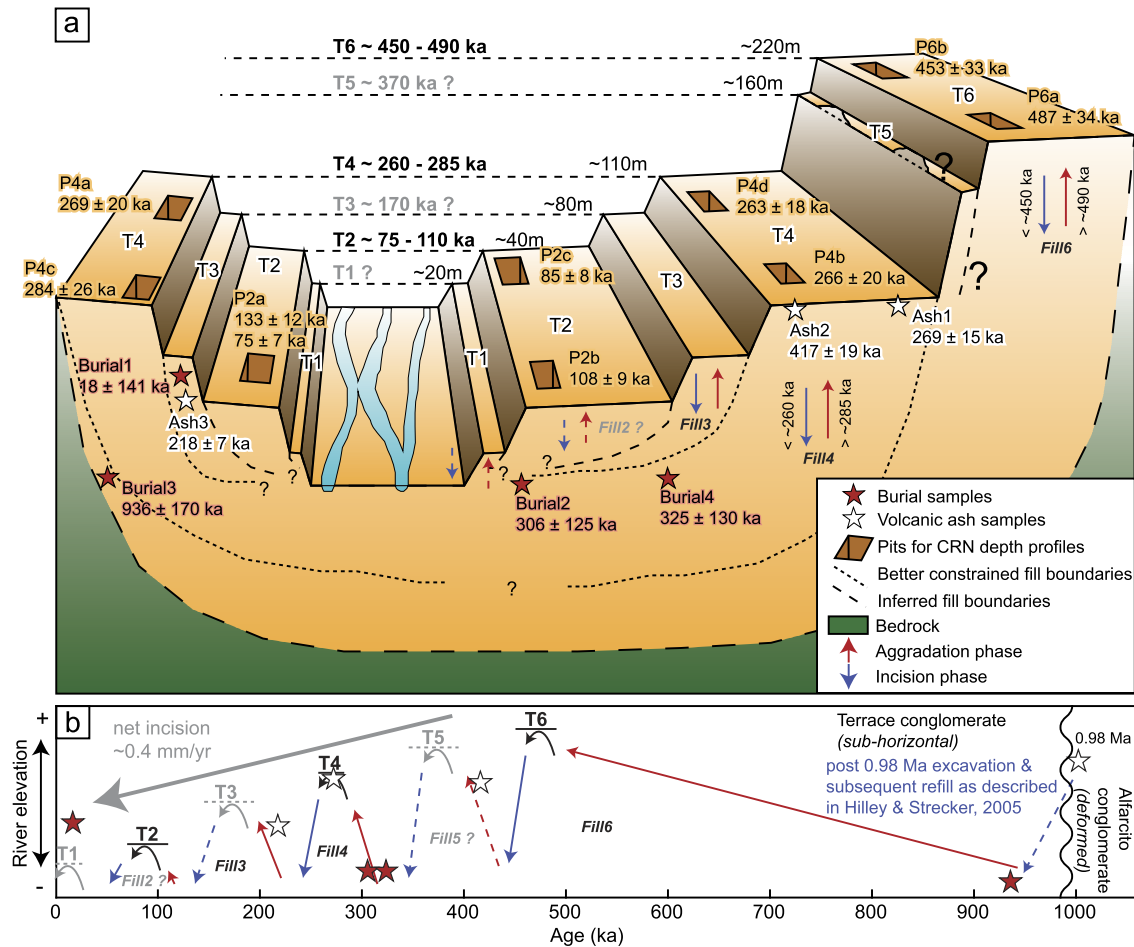


**Fig. 5.** Simplified overview of the spatial sample distribution and the temporal evolution of the fill terraces. (a) Schematic block diagram across the Toro Basin illustrating the relative locations of Pleistocene fluvial terraces and our samples. Ages on the dashed lines in the back indicate terrace age ranges based on the depth profiles (black) and predicted ages for undated terraces (grey). Height numbers give the approximate elevation of the terrace treads above the modern channel. (b) Temporal evolution of the Toro Basin and relative locations of our samples. Solid red and blue lines indicate better constrained aggradation and incision phases, while dashed lines indicate inferred phases of river elevation change. The equivalent fill units are numbered in accordance and distinguished between better constrained (black) and inferred (grey). 0.98 Ma volcanic ash in the upper Alfarficio conglomerate from Marrett et al. (1994).

with the *Stable-surface* ages. Because the age distribution suggests that inflation has raised the terrace surfaces by several 10s of cm with respect to the underlying material, with a consequent large influence on exposure-age calculations, we consider the ages derived from the *Surface-pebbles* approach (which is insensitive to surface inflation) to be more reliable. For P4d, two ages with different inheritance concentrations were generated ( $190 \pm 14$  ka and  $263 \pm 18$  ka). Because P4d is located on the same terrace level as P4a and P4c with calculated ages of  $269 \pm 20$  ka and  $284 \pm 26$  ka, we consider the calculated age for P4d of  $263 \pm 18$  ka (based on P4a inheritance concentrations) to be more reliable.

For the two sand profiles (P2a, P4b), the age determination is limited to the depth-profile calculations, since we cannot apply the *Surface-pebbles* approach. Because the *Inflation-corrected* approach ages of the pebble profiles correlate better with the *Surface-pebbles*

ages, we prefer the *Inflation-corrected* age for P4b. For the upper surface of P2a, we could only calculate an age using the *Stable-surface* approach, because no obvious sand/silt layer is visible. Following these choices (bold ages in Table 1), we obtain preferred exposure ages of ca. 75 to 110 ka for the lowermost dated terrace surface (T2), ca. 260 to 285 ka for T4, and ca. 450 to 490 ka for T6 (Fig. 5a).

We assume that the exposure ages of the terrace treads are equivalent to the time of terrace abandonment associated with the onset of incision. The three dated terraces (T2, T4, and T6) are separated by ca. 200 kyr and the presence of two terraces of unknown age in between (T3 and T5) suggests the formation of one terrace every  $\sim 100$  kyr. Consequently, we infer an abandonment age of ca. 170 ka for T3 and ca. 370 ka for T5.

## 5.2. Cut-and-fill cycles within the Toro Basin

Sometime after 0.98 Ma, the Toro Basin experienced incision to a base-level similar to today, followed by a major phase of aggradation related to basement block uplift in the lower part of the Basin (see section 2.1 and Fig. 2b, Hilley and Strecker, 2005). The age constraint is based on a 0.98 Ma ash (Marrett et al., 1994) that is incorporated into the deformed uppermost Alfarcito conglomerate, which is unconformably overlain by the undeformed Terrace Conglomerates (Fig. 5b). Although Hilley and Strecker (2005) suggested that this aggradation was followed by episodic incision with no intervening filling phases to create the terraces, the position of our samples in the stratigraphy and our  $^{26}\text{Al}/^{10}\text{Be}$  burial and U–Pb zircon ages (ranging from  $18 \pm 141$  ka to  $936 \pm 170$  ka) preclude the possibility of a single fill unit that was episodically incised. Instead, our results imply several cut-and-fill events. We do not have age constraints for the fill beneath each terrace tread. Fill units are named according to the terrace tread that lies above it (e.g., *Fill6* lies beneath T6) and based on their ages, we assign each CRN burial and ash sample to one fill unit.

The oldest fill unit (*Fill6*) is defined by the age of *Burial3* ( $936 \pm 170$  ka), which was collected from an undeformed conglomerate ~15 m above the current main channel (Fig. 5b). Hence, at around 940 ka, the elevation of the upper reaches of the Río Toro was locally almost as deep as today, and more than 200 m of net aggradation occurred before the formation of the highest dated terrace (T6) at ca. 450 to 490 ka. We have no time constraints on the abandonment of T5 (although we predict it to be around 370 ka), nor do we know if a separate fill unit (*Fill5*) underlies it.

The next aggradation phase (*Fill4*) is dated by the CRN burial samples *Burial2* ( $306 \pm 125$  ka) and *Burial4* ( $325 \pm 130$  ka), which were collected ~15 to 20 m above the current river level, implying that the river elevation at ~300 ka, between the abandonment of T5 and aggradation to T4, was at least as low as it is today. These sites were recently exposed due to undercutting by the Río Toro, and thus time for post-depositional CRN production has been short. Similarities in elevation and age imply that both conglomerates belong to a single aggradation phase shortly before the abandonment of T4 (260–285 ka).

The ash layer *Ash1* ( $269 \pm 15$  ka), sampled from *Fill4* 30 cm below the T4 tread, corresponds closely to the surface-abandonment age of T4 (ca. 260–285 ka), indicating that the ash was deposited on the floodplain shortly before the river system switched from aggradation to incision. *Ash2* was sampled within P4b at ~50–60 cm below the T4 tread and yielded an age of  $417 \pm 38$  ka, which is considerably older than the terrace tread above it (260–285 ka) and also older than *Ash1*, which was deposited at a similar stratigraphic level. Because we interpret *Ash2* to be re-worked and less pronounced than *Ash1*, its age only provides an upper limit to the depositional age of *Fill4*.

The next aggradation phase (*Fill3*) is constrained by *Ash3* ( $218 \pm 14$  ka), which we correlate with the fill deposit below T3 based on its elevation. This ash limits the abandonment age of terrace T3 to <218 ka (undated, but inferred to be ~170 ka). Stratigraphically, *Burial1*, which yielded an age of  $18 \pm 141$  ka, belongs to the same fill unit as *Ash2* and should therefore be older than the surface-abandonment age of the T3 terrace (estimated to be ca. 170 ka). *Burial1* was collected from a vertical wall (Fig. S1) 60 m above the current channel. As such, some post-depositional nuclide production may have occurred since the river first exposed the outcrop, which would reduce the burial age and may explain why it overlaps with the present day within uncertainty. Although the  $2\sigma$  age uncertainty also overlaps with the inferred abandonment age of T3, to avoid confusion, we omit this sample from further discussion.

We find no younger depositional ages documenting another fill unit (a hypothetical *Fill2*). However, an additional incision phase

is marked by the abandonment of terrace T2 between ca. 75 and 110 ka based on the depth profiles P2a, P2b and P2c (bold ages in Table 1).

Together, the CRN burial ages, the volcanic-ash ages, and the terrace-abandonment ages suggest that the terraces formed as a result of multiple cut-and-fill cycles. Based on the limited number of burial and ash ages obtained, we suggest a minimum of three principal phases of aggradation (solid red arrows in Fig. 5b); however, more filling phases – potentially one related to each terrace – are possible. Currently, we cannot determine whether there was (a) an overall reduction of the cut-and-fill amplitude (Fig. 5b), or if (b) younger incision events have cut deeper below the present river level. Nevertheless, we observe net incision at a rate of about 0.4 mm/yr based on the decreasing tread heights since the formation of the T6 surface (Fig. 5b and Fig. S4).

## 5.3. Potential causes of terrace formation

The formation of fluvial terraces associated with ~100 kyr cut-and-fill cycles indicates significant changes in sediment supply and/or runoff within the Toro Basin. Below, we discuss the potential roles of (a) autogenic forcing, (b) tectonics, and (c) climate as potential drivers of sediment filling and excavation within the Toro Basin.

### 5.3.1. Autogenic forcing

External perturbation of a fluvial system does not necessarily result in the formation of a single terrace, but rather can lead to autogenic terrace formation, in which several waves of bed-elevation change form a flight of terraces (e.g., Schumm and Parker, 1973). In this case, the highest terrace is created by the initial perturbation, while subsequent feedback mechanisms between the main channel and tributaries induce alternations between aggradation and incision and thus generate additional, lower fill terraces. In the field, we did not find any evidence for such major perturbations related to river capture or landslides voluminous enough to explain hundreds of meters of aggradation over timescales of  $10^4$  to  $10^5$  years. However, a perturbation at the outlet of the Río Toro could have been possible. After exiting the basin, the Río Toro crosses the alluvial fan in the Lerma Valley and today drains into the Cabra Corral reservoir (~1030 m asl) at the southeastern border of the basin (Fig. 2a). Lacustrine deposits in the Lerma Valley indicate the existence of the Pleistocene 'Lake Lerma' (most likely between 0.78–0.1 Ma) with a highstand  $\leq 170$  m above the current Cabra Corral level (Malamud et al., 1996). However, a single major lake-level drop of 170 m can still not explain multiple fill thicknesses of at least 220 m in the upper sectors of the Toro Basin.

### 5.3.2. Tectonic forcing

Hilley and Strecker (2005) related the onset of deposition of the Terrace Conglomerates within the Toro Basin (<0.98 Ma) to the reactivated uplift of the Sierra de Pascha Sur, which would have caused steepening of the river channel within the gorge and deposition upstream of the Gólgota Fault (Fig. 2b). Since the formation of T6 (ca. 450 to 490 ka), we observe net fluvial incision of the Terrace Conglomerates with multiple superimposed cut-and-fill cycles. A purely local tectonic explanation for this landscape would require a cyclically changing uplift rate of the Sierra de Pascha Sur. Although such changes are difficult to envisage, the terrace region could also be influenced by changes in base-level in the Lerma Valley, assuming that these signals can propagate upstream. There is evidence for tectonically induced long-term rock uplift as well as base-level rise in the region (García et al., 2013; Hilley and Strecker, 2005) both of which should affect river incision and aggradation.

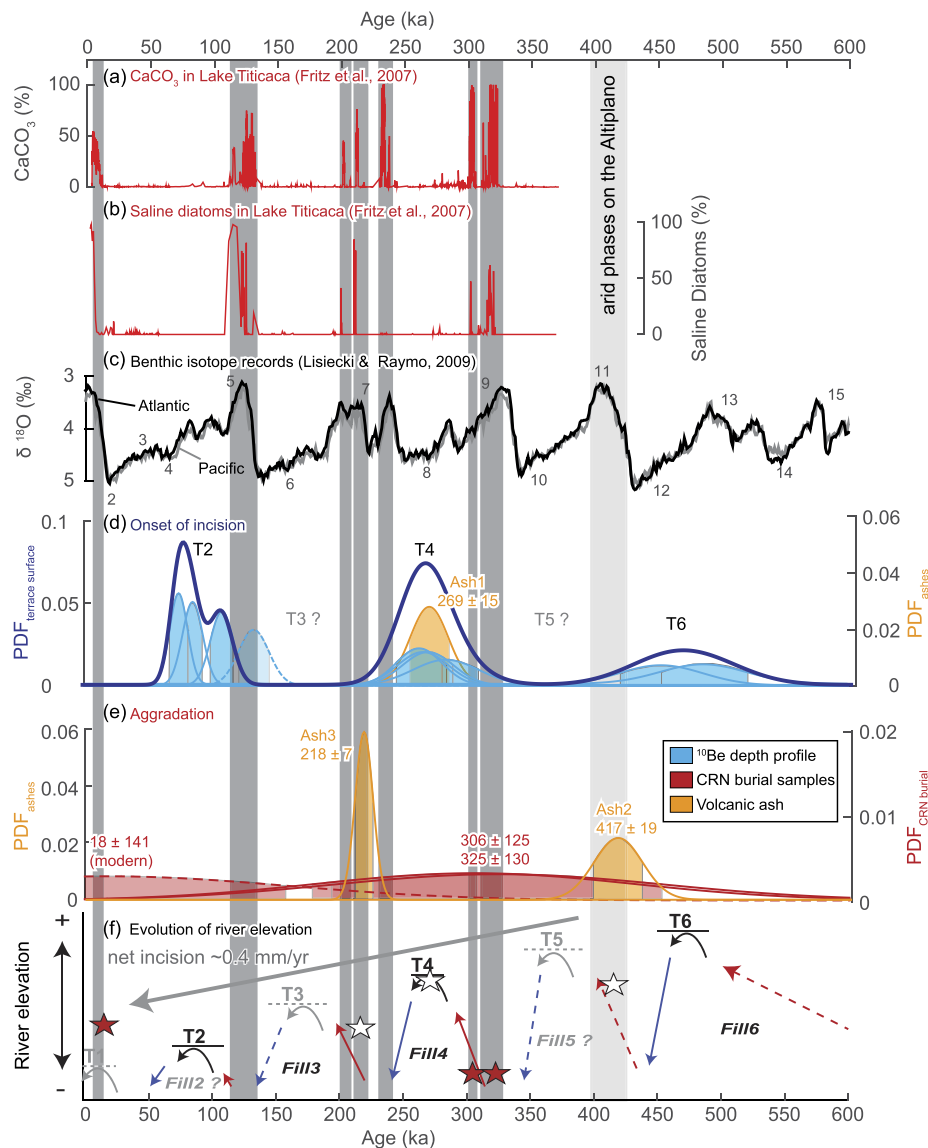


**Fig. 6.** Comparison of aggradation and incision phases in the Toro Basin with regional and global climate proxies.  $\text{CaCO}_3$  concentrations (a) and saline diatom abundance (b) in a Lake Titicaca sediment core (Fritz et al., 2007). High values of both indicate arid phases, which are marked by the grey bars. (c) Average benthic isotope records for the Atlantic (black) and Pacific (grey) oceans (Lisiecki and Raymo, 2009). Numbers indicate Marine Isotope Stages (MIS). (d) Probability density functions (PDF) of the nine terrace surface abandonment ages (light blue) based on the  $^{10}\text{Be}$  depth profiles as indicated in bold in Table 1 and a stacked PDF to show the overall trend of onset of incision (dark blue). Dashed line represents the lower, buried unit of P2a and is not included in the stacked PDF. Based on its location close to a confluence, we consider this lower unit as a period of no deposition and later re-occupation rather than the onset of a major incision phase. Additionally, the PDF of Ash1, which was deposited on the floodplain shortly before incision must have started, is plotted in orange. (e) PDFs of the CRN burial (red) and volcanic ash (orange) ages that represent times of deposition. Note the different y-axis for the CRN burial and volcanic ash ages for better visibility. The shaded areas in (d) and (e) represent the  $1\sigma$  uncertainty ranges. (f) Approximate evolution of river elevation (same as Fig. 5b).

Uplift of the Mojotoro range, which bounds the Lerma Valley to the east (Fig. 2a), started at 10 to 5 Ma, and contributed to several hundred meters of surface uplift during the Quaternary (García et al., 2013; Hain et al., 2011). This enhancement of orographic shielding likely reduced precipitation and fluvial-transport capacity within the hinterland basins (Hain et al., 2011). Although no evidence was found for sustained internal drainage of the Lerma Valley on longer timescales (Hain et al., 2011), the reduced fluvial connectivity to the foreland and associated transient sediment storage is expressed in a 300 m elevation difference between the Lerma Valley and the lower, adjacent basin to the east (Hain et al., 2011). Thus, the overall rise in base-level elevation in the Lerma Valley could also have promoted sediment aggradation in the Toro Basin, but its timing is poorly constrained.

We cannot differentiate whether the onset of net incision of the Terrace Conglomerates at ca. 500 ka was related to changes in tectonic uplift rates or a decrease in the  $Q_s/Q_w$  ratio in the Toro Basin. The net incision rate of  $\sim 0.4$  mm/yr in the terrace region (Fig. 5b and Fig. S4) correlates well with reported long-term uplift rates of the eastern bounding and adjacent ranges, which range from 0.4 to 0.6 mm/yr (Sierra de Pascha, Hilley and Strecker, 2005) and from 0.3 to 1.0 mm/yr (Cordon de Lesser, García et al., 2013). This correspondence could mean that the region of the river terraces has experienced a similar uplift rate, and that net river incision is keeping pace with that uplift. Alternatively, a slowing of the uplift rate of the Sierra de Pascha Sur could have driven net incision in the terrace region, but at a rate that is difficult to predict. Through either mechanism, the tectonic activity of the region could explain the net incision of the Toro Basin since at least ca. 500 ka.

However, the cyclical alternations between aggradation and incision on  $\sim 100$  kyr timescales likely requires an additional driver.

### 5.3.3. Climate forcing

Another mechanism to trigger fluvial incision or aggradation is by changing the incoming  $Q_s/Q_w$  ratio (Parker, 1998). Because the Toro Basin has a virtually unlimited supply of sediment in the form of unlithified fluvial conglomerate, the influence of climate on terrace formation and fluvial long-profile evolution may be primarily associated with past variability in  $Q_w$ . Unfortunately, there is no paleoclimate record from the nearby Puna that is sufficiently old to compare with our terrace sequence. However, there is one terrestrial paleo-climate record from the Altiplano based on a drill core from Lake Titicaca (Fig. 1b), whose  $\text{CaCO}_3$  content (Fig. 6a) and diatoms with saline affinity (Fig. 6b) show a dominant 100 kyr cyclicity in humidity (Fritz et al., 2007). A comparison of our terrace exposure,  $^{26}\text{Al}/^{10}\text{Be}$  burial, and volcanic ash ages to temporal trends in the Lake Titicaca records shows that the onsets of the three dated incision phases (i.e., terrace-abandonment ages; Fig. 6d) correlate with wetter phases in the Lake Titicaca region. We plotted *Ash1* together with the terrace surface abandonment ages (Fig. 6d) because that sample was collected a few cm below the surface of T4, and must have been deposited on the floodplain shortly before incision started. Conversely, the episodes of deposition (Fig. 6e) occur during arid phases ( $\sim 218$  ka,  $\sim 306$ – $325$  ka, and  $\sim 417$  ka). Aggradation of the Río Toro today, during the present arid interglacial, corroborates this pattern (Fig. 2b). Furthermore, a comparison with global benthic oxygen isotope records (Fig. 6c, Lisiecki and Raymo, 2009) implies that the onset of terrace abandonment phases correlates with transitions into global glacial stages. Wetter conditions in the Central Andes due to increased precipitation and/or reduced evapotranspiration during glacial times have commonly been inferred from field studies (Baker and Fritz, 2015; Fritz et al., 2007; Haselton et al., 2002) and modeling studies (Vizy and Cook, 2007). As a result, the fluvial transport capacity in the Toro Basin may have increased during glacial phases more than the sediment flux did. In contrast, during the warm, arid phases, the transport capacity would have been reduced, resulting in an increase in the  $Q_s/Q_w$  ratio and aggradation (e.g., Hanson et al., 2006). Overall, we suggest that while post-500-ka net incision of the Toro Basin is likely controlled by regional tectonic activity, the superimposed 100 kyr aggradation-incision cycles are climate-driven and have been caused by changes in the  $Q_s/Q_w$  ratio.

### 5.4. Impacts of global climate change on sedimentary systems

Although fluvial terraces in the Central Andes have commonly been linked to moisture fluctuations within the past  $\sim 100$  kyr (e.g. Farabaugh and Rigsby, 2005; Schildgen et al., 2016; Steffen et al., 2010; Tchilinguirian and Pereyra, 2001), the only other record of Andean fluvial terraces that span multiple 100 kyr glacial cycles is from the southernmost Central Andes (Río Diamante, Fig. 1b), where Baker et al. (2009) correlated the deposition of fluvial fill units with glacial advances. Globally, the formation of fluvial terraces related to 100 kyr glacial–interglacial cycles has also been shown in the Tian Shan (Huang et al., 2014), on the NE Tibetan Plateau (Pan et al., 2003), in the Apennines (Wegmann and Pazzaglia, 2009), and in several locations within Europe (Bridgland and Westaway, 2008).

But why have 100 kyr cycles in terrace formation only been reported in one other location in the Andes (Río Diamante), despite the large number of existing terrace studies? Our knowledge of how periodic forcing signals are preserved in sedimentary records is limited and mainly based on numerical models (e.g. Braun et al., 2015; Castellort and Van Den Driessche, 2003;

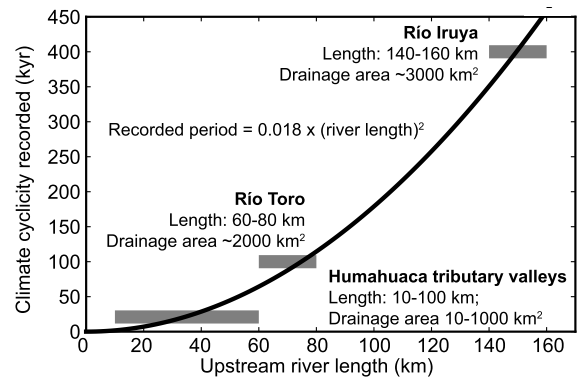


Fig. 7. Correlation of recorded climate cyclicity and river length. Three sedimentary records from the eastern flank of the southern Central Andes (Fisher et al., 2016; Schildgen et al., 2016; this study) preserve paleoclimate cycle periodicities that are proportional to the square of river length upstream of their depositional area, consistent with the linear-diffusional model of Castellort and Van Den Driessche (2003).

Godard et al., 2013). It has been suggested that if the response time of the alluvial long profile is longer than the periodicity of the forcing, changes in sediment export efficiency will be buffered and will not lead to a morphological response (Allen, 2008). Castellort and Van Den Driessche (2003) proposed that diffusive waves of sediments in alluvial systems lead to a perturbation response time that is proportional to a representative transport distance squared, following the linear diffusive model of Paola et al. (1992). This result contrasts with the length scale-independent response to climate change described by Braun et al. (2015), whose landscape evolution model includes stream power based channel erosion and hillslope diffusion, but does not explicitly model sediment transport through the river system.

Although we cannot explain with certainty why the geomorphic record in Toro Basin is dominated by 100 kyr climate cyclicity, a correlation between catchment length scales and recorded climate periodicity exists throughout the southern Central Andes. For example, late Quaternary fluvial deposits in tributary valleys within the Humahuaca Basin (Fig. 1c) record changes associated with precessional (21 kyr) cyclicity from catchments ranging in length from 10 to 100 km (Schildgen et al., 2016), whereas Pliocene to late Pleistocene deposits in the  $\sim 140$ – $160$  km long Río Iruya (Fig. 1c) record long-eccentricity (400 kyr) cyclicity (Fisher et al., 2016). For comparison, the river length upstream from the terraces in the Toro Basin is  $\sim 60$ – $80$  km. A simple curve-fit, albeit with only three river systems (Fig. 7), provides empirical support for the length-scale-dependent fluvial response time in alluvial rivers (e.g. Castellort and Van Den Driessche, 2003). Hence, although river length is likely not the only factor affecting fluvial response times, these three drainage systems in NW Argentina offer compelling evidence of how different periodicities of climate forcing can be preserved in geomorphic archives at differing distances from their source areas.

## 6. Conclusions

Three terrace abandonment ages in the Toro Basin of NW Argentina calculated from nine *in situ*  $^{10}\text{Be}$  depth profiles range from  $75 \pm 7$  to  $487 \pm 34$  ka and reveal an apparent 100 kyr cyclicity in the formation of six terraces. Additional dating of sediment deposition, based on cosmogenic burial samples and volcanic ashes, suggest the terraces result from multiple cut-and-fill cycles. The initial filling of the extensive Terrace Conglomerate within the Toro Basin is most likely linked to basement uplift near the catchment outlet, beginning at  $\sim 1$  Ma. Either (1) changes in uplift rate of this basement block or (2) regional rock uplift could explain the net

incision of the Río Toro since ca. 500 ka. However, the superimposed 100 kyr aggradation and incision cycles are best explained by climate forcing. Preservation of these cycles likely results from a fortuitous combination of enhanced preservation potential in a region of long-term net incision together with river response times (potentially linked to channel length) that are appropriate for recording 100 kyr cyclic forcing. The times of river incision onset correlate with wetter phases recorded in a Lake Titicaca sediment core, whereas depositional phases mainly fall within arid periods. Increased moisture availability in the southern Central Andes has been previously shown to coincide with global glacial cycles. We suggest that enhanced precipitation and/or reduced evapotranspiration during global cold phases resulted in increased water discharge and sediment transport capacity in the Río Toro and its tributaries, which outweighed any increases in sediment flux in this transport-limited system and thus triggered river incision.

### Acknowledgements

This study was funded by the Emmy-Noether-Programme of the Deutsche Forschungsgemeinschaft (DFG) grant number SCHI 1241/1-1 awarded to T. Schildgen. M. Strecker acknowledges DFG funding (grant number STR 373/32-1, StRATEGy). We thank George Hilley for providing data from the sampling campaign he performed in 2003, and Walter Düsing for field assistance. Jan Schüürmann, Lilian Pollozek, David Käter, Martin Lang, and Cathrin Schulz are thanked for their help during sample processing and Steve Binnie and Stefan Heinze for performing the AMS measurements. We thank Luca Malatesta and one anonymous reviewer for their very detailed and constructive reviews that helped to improve the manuscript.

### Appendix A. Supplementary material

Supplementary material related to this article can be found online at <http://dx.doi.org/10.1016/j.epsl.2017.06.001>.

### References

- Allen, P.A., 2008. Time scales of tectonic landscapes and their sediment routing systems. In: *Landsc. Evol. Denudation, Clim. Tectonics over Differ. Time Sp. Scales*, vol. 296, pp. 7–28.
- Anderson, R.S., Repka, J.L., Dick, G.S., 1996. Explicit treatment of inheritance in dating depositional surfaces using *in situ*  $^{10}\text{Be}$  and  $^{26}\text{Al}$ . *Geology* 24, 47–51.
- Baker, P., Fritz, S.C., 2015. Nature and causes of quaternary climate variation of tropical South America. *Quat. Sci. Rev.* 124, 31–47.
- Baker, S.E., Gosse, J.C., McDonald, E.V., Evenson, E.B., Martínez, O., 2009. Quaternary history of the piedmont reach of Río Diamante, Argentina. *J. South Am. Earth Sci.* 28, 54–73. <http://dx.doi.org/10.1016/j.jsames.2009.01.001>.
- Balco, G., Shuster, D.L., 2009.  $^{26}\text{Al}$ - $^{10}\text{Be}$ - $^{21}\text{Ne}$  burial dating. *Earth Planet. Sci. Lett.* 286, 570–575. <http://dx.doi.org/10.1016/j.epsl.2009.07.025>.
- Balco, G., Stone, J.O., Lifton, N.A., Dunai, T.J., 2008. A complete and easily accessible means of calculating surface exposure ages or erosion rates from  $^{10}\text{Be}$  and  $^{26}\text{Al}$  measurements. *Quat. Geochronol.* 3, 174–195.
- Blard, P.-H., Braucher, R., Lavé, J., Bourlès, D.L., 2013. Cosmogenic  $^{10}\text{Be}$  production rate calibrated against  $^3\text{He}$  in the high Tropical Andes (3800–4900 m, 20–22°S). *Earth Planet. Sci. Lett.* 382, 140–149. <http://dx.doi.org/10.1016/j.epsl.2013.09.010>.
- Bobst, A.L., Lowenstein, T.K., Jordan, T.E., Godfrey, L.V., Ku, T.-L., Luo, S., 2001. A 106 ka paleoclimate record from drill core of the Salar de Atacama, northern Chile. *Palaeogeogr. Palaeoclimatol. Palaeoecol.* 173, 21–42.
- Bookhagen, B., Strecker, M.R., 2008. Orographic barriers, high-resolution TRMM rainfall, and relief variations along the eastern Andes. *Geophys. Res. Lett.* 35 (6). <http://dx.doi.org/10.1029/2007GL032011>.
- Braun, J., Voisin, C., Gourlan, A.T., Chauvel, C., 2015. Erosional response of an actively uplifting mountain belt to cyclic rainfall variations. *Earth Surf. Dyn.* 3, 1–14. <http://dx.doi.org/10.5194/esurf-3-1-2015>.
- Bridgland, D., Westaway, R., 2008. Climatically controlled river terrace staircases: a worldwide Quaternary phenomenon. *Geomorphology* 98, 285–315.
- Broccoli, A.J., Dahl, K.A., Stouffer, R.J., 2006. Response of the ITCZ to Northern Hemisphere cooling. *Geophys. Res. Lett.* 33, 1–4. <http://dx.doi.org/10.1029/2005GL024546>.
- Castelltort, S., Van Den Driessche, J., 2003. How plausible are high-frequency sediment supply-driven cycles in the stratigraphic record? *Sediment. Geol.* 157, 3–13. [http://dx.doi.org/10.1016/S0037-0738\(03\)00066-6](http://dx.doi.org/10.1016/S0037-0738(03)00066-6).
- Castino, F., Bookhagen, B., Strecker, M.R., 2016. Rainfall variability and trends of the past six decades (1950–2014) in the subtropical NW Argentine Andes. *Clim. Dyn.*, 1–19. <http://dx.doi.org/10.1007/s00382-016-3127-2>.
- Chmeleff, J., von Blanckenburg, F., Kossert, K., Jakob, D., 2010. Determination of the  $^{10}\text{Be}$  half-life by multicollector ICP-MS and liquid scintillation counting. *Nucl. Instrum. Methods Phys. Res., Sect. B, Beam Interact. Mater. Atoms* 268, 192–199. <http://dx.doi.org/10.1016/j.nimb.2009.09.012>.
- Farabaugh, R.L., Rigsby, C.A., 2005. Climatic influence on sedimentology and geomorphology of the Río Ramis valley, Peru. *J. Sediment. Res.* 75, 12–28.
- Fisher, G.B., Amidon, W.H., Burbank, D.W., Luna, L.V., 2016. Late Miocene to Early Pleistocene paleo-erosion rates and provenance change in the NE Argentinian Andes: apparent coupling of sediment fluxes with 400-kyr eccentricity cycles. *EGU Gen. Assem. Conf. Abstr.* 18, 5310.
- Fritz, S.C., Baker, P.A., Ekdahl, E., Seltzer, G.O., Stevens, L.R., 2010. Millennial-scale climate variability during the Last Glacial period in the tropical Andes. *Quat. Sci. Rev.* 29, 1017–1024. <http://dx.doi.org/10.1016/j.quascirev.2010.01.001>.
- Fritz, S.C., Baker, P.A., Lowenstein, T.K., Seltzer, G.O., Rigsby, C.A., Dwyer, G.S., Tapia, P.M., Arnold, K.K., Ku, T.-L., Luo, S., 2004. Hydrologic variation during the last 170,000 years in the southern hemisphere tropics of South America. *Quat. Res.* 61, 95–104.
- Fritz, S.C., Baker, P.A., Seltzer, G.O., Ballantyne, A., Tapia, P., Cheng, H., Edwards, R.L., 2007. Quaternary glaciation and hydrologic variation in the South American tropics as reconstructed from the Lake Titicaca drilling project. *Quat. Res.* 68, 410–420.
- García, V.H., Hongn, F., Cristallini, E.O., 2013. Late Miocene to recent morphotectonic evolution and potential seismic hazard of the northern Lerma valley: clues from Lomas de Medeiros, Cordillera Oriental, NW Argentina. *Tectonophysics* 608, 1238–1253. <http://dx.doi.org/10.1016/j.tecto.2013.06.021>.
- Godard, V., Tucker, G.E., Burch Fisher, G., Burbank, D.W., Bookhagen, B., 2013. Frequency-dependent landscape response to climatic forcing. *Geophys. Res. Lett.* 40, 859–863. <http://dx.doi.org/10.1002/grl.50253>.
- Godfrey, L.V., Jordan, T.E., Lowenstein, T.K., Alonso, R.L., 2003. Stable isotope constraints on the transport of water to the Andes between 22° and 26°S during the last glacial cycle. *Palaeogeogr. Palaeoclimatol. Palaeoecol.* 194, 299–317.
- Gosling, W.D., Bush, M.B., Hanselman, J.A., Chepstow-Lusty, A., 2008. Glacial-interglacial changes in moisture balance and the impact on vegetation in the southern hemisphere tropical Andes (Bolivia/Peru). *Palaeogeogr. Palaeoclimatol. Palaeoecol.* 259, 35–50. <http://dx.doi.org/10.1016/j.palaeo.2007.02.050>.
- Granger, D.E., Muzikar, P.F., 2001. Dating sediment burial with *in situ*-produced cosmogenic nuclides: theory, techniques, and limitations. *Earth Planet. Sci. Lett.* 188, 269–281. [http://dx.doi.org/10.1016/S0012-821X\(01\)00309-0](http://dx.doi.org/10.1016/S0012-821X(01)00309-0).
- Hain, M.P., Strecker, M.R., Bookhagen, B., Alonso, R.N., Pingel, H., Schmitt, a.K., 2011. Neogene to Quaternary broken foreland formation and sedimentation dynamics in the Andes of NW Argentina (25°S). *Tectonics* 30 (2). <http://dx.doi.org/10.1029/2010TC002703>.
- Hanson, P.R., Mason, J.A., Goble, R.J., 2006. Fluvial terrace formation along Wyoming's Laramie range as a response to increased late Pleistocene flood magnitudes. *Geomorphology* 76, 12–25. <http://dx.doi.org/10.1016/j.geomorph.2005.08.010>.
- Haselton, K., Hilley, G., Strecker, M.R., 2002. Average pleistocene climatic patterns in the Southern Central Andes: controls on mountain glaciation and paleoclimate implications. *J. Geol.* 110, 211–226. <http://dx.doi.org/10.1086/338414>.
- Hidy, A.J., Gosse, J.C., Pederson, J.L., Mattern, J.P., Finkel, R.C., 2010. A geologically constrained Monte Carlo approach to modeling exposure ages from profiles of cosmogenic nuclides: an example from Lees Ferry, Arizona. *Geochim. Geophys. Geosyst.* 11. <http://dx.doi.org/10.1029/2010GC003084>.
- Hilley, G.E., Strecker, M.R., 2005. Processes of oscillatory basin filling and excavation in a tectonically active orogen: Quebrada del Toro Basin, NW Argentina. *Bull. Geol. Soc. Am.* 117, 887–901. <http://dx.doi.org/10.1130/B25602.1>.
- Huang, W.L., Yang, X.P., Li, A., Thompson, J.A., Zhang, L., 2014. Climatically controlled formation of river terraces in a tectonically active region along the southern piedmont of the Tian Shan, NW China. *Geomorphology* 220, 15–29. <http://dx.doi.org/10.1016/j.geomorph.2014.05.024>.
- Huntington, E., 1907. Some characteristics of the glacial period in non-glaciated region. *Bull. Geol. Soc. Am.* 18, 351–388.
- Lal, D., 1991. Cosmic ray labeling of erosion surfaces: *in situ* nuclide production rates and erosion models. *Earth Planet. Sci. Lett.* 104, 424–439. [http://dx.doi.org/10.1016/0012-821X\(91\)90220-C](http://dx.doi.org/10.1016/0012-821X(91)90220-C).
- Liseicki, L.E., Raymo, M.E., 2009. Diachronous benthic  $\delta^{18}\text{O}$  responses during late Pleistocene terminations. *Paleoceanography* 24, 1–14. <http://dx.doi.org/10.1029/2009PA001732>.
- Malamud, B.D., Jordan, T.E., Alonso, R.A., Gallardo, E.F., González, R.E., Kelley, S.A., 1996. Pleistocene Lake Lerma, Salta Province, NW Argentina. Present the XIII Congr. Geológico Argentino, pp. 103–116.
- Marrett, R.A., Allmendinger, R.W., Alonso, R.N., Drake, R.E., 1994. Late Cenozoic tectonic evolution of the Puna Plateau and adjacent foreland, northwestern Argentine Andes. *J. South Am. Earth Sci.* 7, 179–207.

- Marrett, R., Strecker, M.R., 2000. Response of intracontinental deformation in the central Andes to late Cenozoic reorganization of South American Plate motions. *Tectonics* 19, 452–467.
- McFadden, L.D., Wells, S.G., Jercinovich, M.J., 1987. Influences of eolian and pedogenic processes on the origin and evolution of desert pavements. *Geology* 15, 504–508.
- Nishiizumi, K., 2004. Preparation of  $^{26}\text{Al}$  AMS standards. *Nucl. Instrum. Methods Phys. Res., Sect. B, Beam Interact. Mater. Atoms* 223, 388–392. <http://dx.doi.org/10.1016/j.nimb.2004.04.075>.
- Pan, B., Burbank, D., Wang, Y., Wu, G., Li, J., Guan, Q., 2003. A 900 k.y. record of strath terrace formation during glacial–interglacial transitions in northwest China. *Geology* 31, 957–960. <http://dx.doi.org/10.1130/G19685.1>.
- Paola, C., Heller, P.L., Angevine, C.L., 1992. The large-scale dynamics of grain-size variation in alluvial basins, 1: theory. *Basin Res.* 4, 73–90. <http://dx.doi.org/10.1111/j.1365-2117.1992.tb00145.x>.
- Parker, G., 1998. Alluvial fans formed by channelized fluvial and sheet flow. I: theory. *J. Hydraul. Eng.*, 985–995. [http://dx.doi.org/10.1061/\(ASCE\)0733-9429\(2000\)126:3\(224.x\)](http://dx.doi.org/10.1061/(ASCE)0733-9429(2000)126:3(224.x)).
- Penck, A., 1884. Über Periodicität der Thalbildung.. *Verhandlung der Gesellschaft für Erdkd. zu Berlin*, pp. 39–59.
- Placzek, C., Quade, J., Patchett, P.J., 2006. Geochronology and stratigraphy of late Pleistocene lake cycles on the southern Bolivian Altiplano: implications for causes of tropical climate change. *Geol. Soc. Am. Bull.* 118, 515–532.
- Schildgen, T.F., Robinson, R.A.J., Savi, S., Phillips, W.M., Spencer, J.Q.G., Bookhagen, B., Scherler, D., Tofelde, S., Alonso, R.N., Kubik, P.W., Binnie, S.A., Strecker, M.R., 2016. Landscape response to late Pleistocene climate change in NW Argentina: sediment flux modulated by basin geometry and connectivity. *J. Geophys. Res., Earth Surf.* 121, 392–414. <http://dx.doi.org/10.1002/2015JF003607>.
- Schumm, S.A., Parker, R.S., 1973. Implication of complex response of drainage systems for Quaternary alluvial stratigraphy. *Nat. Phys. Sci.* 243, 99–100.
- Schwab, K., Schäfer, A., 1976. Sedimentation und Tektonik im mittleren Abschnitt des Río Toro in der Ostkordillere NW-Argentiniens. *Geol. Rundsch.* 65, 175–194. <http://dx.doi.org/10.1007/BF01808462>.
- Steffen, D., Schlunegger, F., Preusser, F., 2010. Late Pleistocene fans and terraces in the Majes valley, southern Peru, and their relation to climatic variations. *Int. J. Earth Sci.* 99, 1975–1989.
- Tchilinguirian, P., Pereyra, F.X., 2001. Geomorfología del sector Salinas Grandes-Quebrada de Humahuaca, provincia de Jujuy. *Rev. Asoc. Geol. Argent.* 56 (1), 3–15.
- Vera, C., Higgins, W., Amador, J., Ambrizzi, T., Garreaud, R., Gochis, D., Gutzler, D., Lettenmaier, D., Marengo, J., Mechoso, C.R., Nogues-Paegle, J., Silva Dias, P.L., Zhang, C., 2006. Toward a unified view of the American monsoon systems. *J. Climate*. <http://dx.doi.org/10.1175/JCLI3896.1>.
- Vizy, E.K., Cook, K.H., 2007. Relationship between Amazon and high Andes rainfall. *J. Geophys. Res., Atmos.* 112, 1–14. <http://dx.doi.org/10.1029/2006JD007980>.
- Wegmann, K.W., Pazzaglia, F.J., 2009. Late Quaternary fluvial terraces of the Romagna and Marche Apennines, Italy: climatic, lithologic, and tectonic controls on terrace genesis in an active orogen. *Quat. Sci. Rev.* 28, 137–165. <http://dx.doi.org/10.1016/j.quascirev.2008.10.006>.
- Zech, J., Zech, R., Kubik, P.W., Veit, H., 2009. Glacier and climate reconstruction at Tres Lagunas, NW Argentina, based on  $^{10}\text{Be}$  surface exposure dating and lake sediment analyses. *Palaeogeogr. Palaeoclimatol. Palaeoecol.* 284, 180–190. <http://dx.doi.org/10.1016/j.palaeo.2009.09.023>.